Structured soil mixture for solving deformation issue in GeoBarrier System

Chua,Yuan Shen; Rahardjo, Harianto; Satyanaga, Alfrendo

2022

Chua, Y. S., Rahardjo, H. & Satyanaga, A. (2022). Structured soil mixture for solving deformation issue in GeoBarrier System. Transportation Geotechnics, 33, 100727-. https://dx.doi.org/10.1016/j.trgeo.2022.100727

https://hdl.handle.net/10356/162175

https://doi.org/10.1016/j.trgeo.2022.100727

Structured Soil Mixture for Solving Deformation Issue in GeoBarrier System

Chua Yuan Shen, Harianto Rahardjo, Alfrendo Satyanaga

[1]Master Student, School of Civil and Environmental Engineering, Nanyang Technological University, Singapore

[2]Professor, School of Civil and Environmental Engineering, Nanyang Technological University, Singapore

[3]Assistant Professor, Department of Civil and Environmental Engineering, Nazarbayev University, 53 Kabanbay Batyr Ave, 010000, Nur-Sultan, Kazakhstan

*Corresponding Author: Harianto Rahardjo; email: chrahardjo@ntu.edu.sg

ABSTRACT:

The GeoBarrier System (GBS) is designed to improve the urban sustainability with the planting bags within it. The GeoBarrier System (GBS) is a man-made 3-layered cover system comprising an exposed vegetative layer combined with hidden 2-layered unsaturated covered system, which harnesses the distinct difference in unsaturated hydraulic properties between a non-cohesive fine-grained layer and a coarse-grained layer. Previous research works indicated that GBS could be used as an earth retaining structure and slope stabilization system against rainfall-induced slope failures. However, the differential settlement was observed along the approved soil mixture (ASM) geobag layers in the previous study. The objective of this project is to investigate the appropriate modification of ASM layers in order to reduce the deformation of planting GeoBags. The research works involved the mixing of ASM with different percentages of recycled concrete aggregate (RCA) (called structured soil mixture or SSM) to improve the modulus elasticity of ASM layer within the planting geobag. The scope of this study includes the laboratory experiments for saturated and unsaturated soil characterization, numerical analyses and loading tests. The results indicated that the soil mixture with a ratio of 50% ASM and 50% coarse RCA can be used to provide improved resistance to deformation of GBS.

KEYWORDS: Geobarrier System; Unsaturated Soil; Approved Soil Mixture; Soil Structure Mixtures; Recycled Concrete Aggregate

1. INTRODUCTION

The GeoBarrier System (GBS) was designed as a resource-efficient innovative alternative to conventional concrete retaining walls, focused towards embracing and supporting sustainable living (Rahardjo et al., 2020). The GBS is a man-made 3-layered cover system (Figure 1) comprising an exposed vegetative layer combined with a hidden 2-layered unsaturated covered system, which harnesses the distinct difference in unsaturated hydraulic properties between a fine-grained layer and a coarse-grained layer (Rahardjo et al., 2019a). The system hinders rainwater from infiltrating into the parent soil beneath, thereby maintaining the slope stability and significantly reducing likelihood of rainfall-induced slope failures. GBS further allows use of recycled material such as recycled concrete aggregates, instead of raw materials, e.g. sand and gravels, to be used as the fine- and coarse-grained layers, thus encouraging recycling. In addition, GBS does not use steel or concrete hence making it more environmentally friendly and cost effective for use in both urban and rural sites. The GBS comes with specially designed planting pockets.

The GBS solution is poised to improve the urban sustainability with the planting bags within it (Rahardjo et al., 2019a). The specially designed planting pockets on the GBS modules, or GeoBags (Figure 2), provide unique opportunity for planting a wide variety of larger ferns, creepers and shrubs which can replace concrete areas with green areas. In line with current sustainable environment policies, recycled materials such as recycled concrete aggregate (RCA) and reclaimed asphalt pavement (RAP) can be used to replace natural aggregates as components of the capillary barrier system (Rahardjo et al. 2013; McCulloch et al. 2017). Previous research works indicated that GBS could be used as earth retaining structure and slope stabilization system against rainfall-induced slope failures (Rahardjo et al., 2016a, b). However, the differential settlement was observed along approved soil mixture (ASM) geobag layers in the previous study. This happened since the ASM layers could not be compacted to high density to allow plant roots to grow within the ASM bag.

Rahardjo et al. (2009) mixed the topsoil or ASM with granite chips to improve the strength of ASM with respect to tree stability. The topsoil used in this research was brown in color and consisted of clayey soil, organic matter (compost), and sand on a volume-basis ratio of 3:2:1, respectively. They observed that a mixture of 50% ASM and 50% granite chip gave a high maximum wind force needed to uproot the tree as indicated by the static analysis and numerical modelling. Rahardjo et al. (2009) also indicated that the use of RCA within ASM did not have negative impact on the plant health.

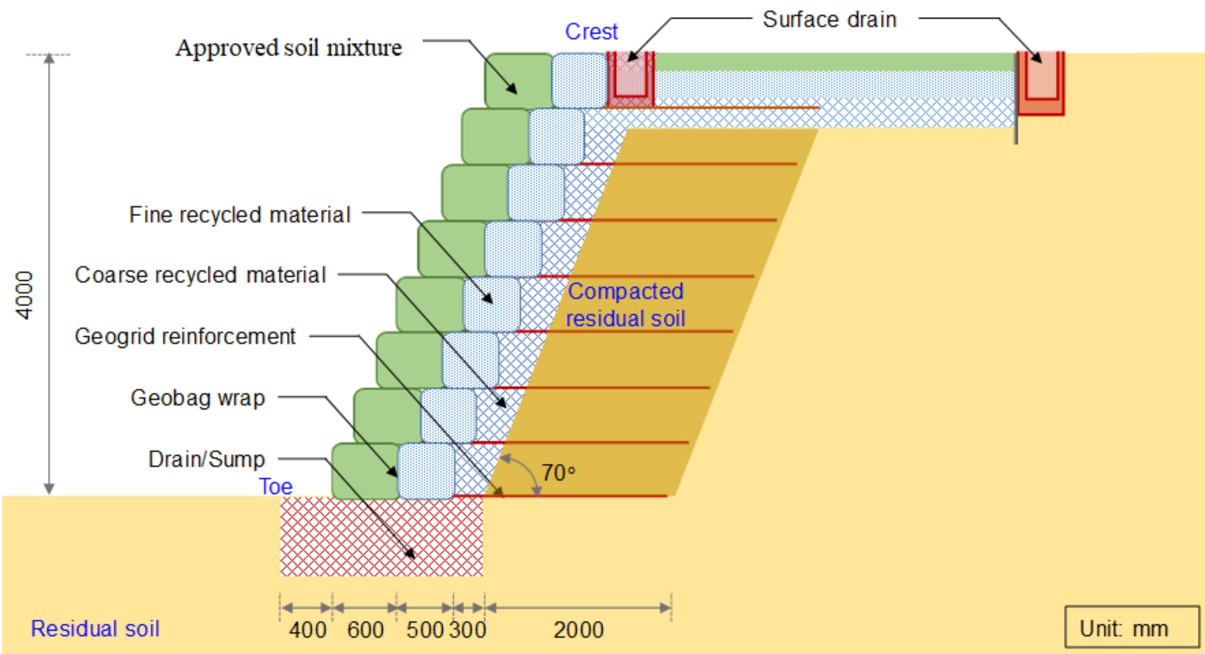

Figure 1. Schematic diagram of Geobarrier System (modified after Rahardjo et al., 2020)

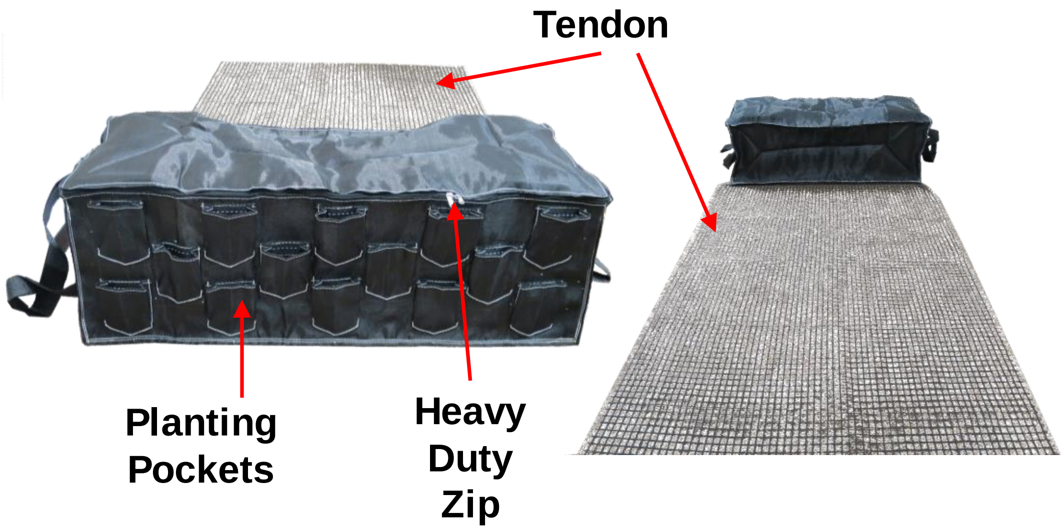

Figure 2. GeoBag with planting pocket

The objective of this study is to investigate the appropriate composition of mixtures between ASM and coarse-grained material to achieve the required allowable deformation within GBS. In addition, the effect of soil mixtures on the saturated and unsaturated soil properties were analyzed in this study. The term used to represent soil mixtures in this study is called Structured Soil Mixture (SSM). The soil mixtures consisted of different percentages of ASM and coarse recycled concrete aggregate (RCA). The study involves the suitability of coarse RCA to replace granite chips, the design of a suitable SSM to replace ASM and laboratory experiments for characterization of saturated and unsaturated properties of SSM with different compositions. The assessment of the performance of GBS incorporating the proposed SSM was carried out using seepage and deformation analyses to observe the water flow characteristics and the deformation characteristics of the proposed SSM under different scenarios. The loading tests were conducted to evaluate the results from deformation analyses.

2. INVESTIGATED MATERIALS

Eight different types of Geobags were investigated in this study with varying dimensions and strengthening materials: 300 mm depth, 400 mm depth, 500 mm depth, 600 mm depth, 500 mm depth with external strap, 600 mm depth with external strap, 500 mm depth with internal straps, 600 mm depth with internal straps. The Geotextile used in this research for manufacturing the GeoBarrier System ASM GeoBags consisted of a woven monofilament fibre weaved to form a stable matrix with high water flow and optimum opening size for soil retention. The specifications of GeoBags are as follows: Tensile strength of greater than or equal to 50 kN/m, California Bearing Ratio (CBR) puncture strength of greater than or equal to 5.0 kN, Pore size of less than or equal to 600 micrometer, Water permeability greater than or equal to 0.2 m/s. The geobags used in this study had the same specifications as used by Rahardjo et al. (2020).

The material used as the external strap was a 70 mm monofilament webbing (with working load of greater than or equal to 3 ton) stitched across the midsection of the Geobag. The material used as the internal strap was a 50 mm monofilament webbing with a working load of greater than or equal to 2 ton. The number of the internal strap for each Geobag was six pcs and each of them was stitched within the Geobag. Three different mixtures of SSM were investigated in this study: 100 % ASM, 80% ASM-20% coarse RCA and 50% ASM-50% coarse RCA. In this study, the ASM was mixed with the RCA with the following compositions: 80% ASM and 20% Coarse RCA (80SSM) and 50% ASM and 50% Coarse RCA (50SSM), on a dry mass basis (Figure 3). The Authors used minimum percentage of ASM (50 %) in the study. The percentage of ASM less than 50 % will affect the plant health (Rahardjo et al., 2019b). The 80% ASM was selected in the soil mixture as median value between 50 % ASM and 100 % ASM. The 100 % ASM was selected as reference in comparison with the other two soil mixtures.

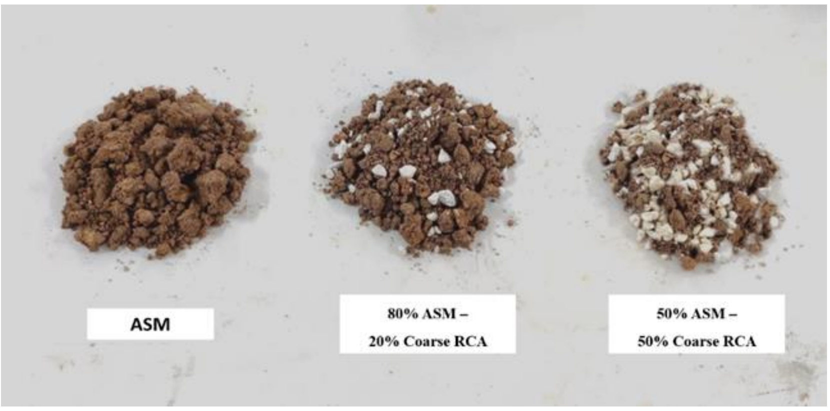

Figure 3. ASM and SSM used in this study

3. METHODOLOGY

This study involves the experimental works in laboratory for characterization of saturated and unsaturated properties of ASM and SSM; finite element seepage and stress-strain analyses; and physical loading test to observe the deformation characteristics of the proposed SSM under different scenarios. Physical loading tests were conducted to observe the deformation characteristics of the proposed SSM under different scenarios. The soil properties from laboratory testing were incorporated in the stress-strain analyses whose results were used to evaluate the results from the loading tests. The seepage analyses were carried out to evaluate the performance of GBS using SSM in minimizing rainwater infiltration into the GBS slope.

3.1 LABORATORY TESTING

Grain-size distributions of the soils were determined following ASTM D6913-04(2009). Specific gravity of the soil mixtures was measured following the procedure described in ASTM D854-02(2002). The soils were classified in accordance with the Unified Soil Classification System (USCS) described in ASTM D 2487-11(2011). Prior to measurements of the soil-water characteristics, saturated permeability and shear strength, the air-dried soils were compacted by tamping under a dry condition (i.e., water content less than 0.5%) to achieve a specified dry density. The dry density corresponds to 90% relative compaction under the standard Proctor effort (ASTM D698-12, 2012). The dry density of each soil was then controlled to be the same for all tests in order to justify the trends of change in the mechanical and hydraulic properties of soils.

The effects of SSM on the SWCCs of the soil mixtures were investigated by conducting Tempe cell tests, as described in Satyanaga and Rahardjo (2020). Procedures of conducting Tempe cell tests at low matric suction values as described in Satyanaga et al. (2017) were adopted in this study. In order to obtain a complete relationship between volumetric water content and matric suction data, the results of the Tempe cell tests were fitted with Fredlund and Xing (1994) function using the correction factor equal to 1 as suggested by Leong and Rahardjo (1997). The saturated permeabilities, k_s, of the ASM and SSM specimens were determined using the falling head method in accordance with Satyanaga et al. (2021). Permeability functions, k_w, of the soils were determined indirectly using the statistical method originally proposed by Childs and Collis George (1950). Statistical method is one of common and most accurate method to determine permeability function as suggested by Zhai et al. (2020, 2019a, 2019b)

The triaxial tests on unsaturated specimens were performed using a conventional triaxial cell that was modified for air and water pressure control (Satyanaga and Rahardjo, 2019b). The axis-translation technique was applied to control the matric suction to the desired values. To facilitate a separate control for the pore-air and pore-water pressures, a 5 bar high-flow high-air entry ceramic disk of 6.35 mm thickness was sealed onto a 10 cm diameter base pedestal that had a circular grooved water compartment. The groove was used to flush diffused air bubbles during the experiments. The required amount of dry soil specimen was placed directly on top of the pre-saturated ceramic disk and was compacted every 1 cm of height to the desired dry density. The compaction method applied in this study was adopted from compaction standards where the soil sample is compacted layer by layer by applying the same compaction effort.

For triaxial tests on saturated specimens, a trial test on saturated ASM showed that a constant axial strain rate of 0.01 mm/min was sufficient for maintaining a constant pore-water pressure during shearing. Therefore, the consolidated drained triaxial tests on saturated soil specimens were carried out at a constant shearing rate of 0.01 mm/ min. For the triaxial tests on unsaturated specimens, the soil specimen was sheared at a constant shearing rate of 0.0009 mm/ min. This axial strain rate had been used for consolidated drained triaxial tests on the residual soil from Singapore (Kim et al., 2021), which had a permeability comparable to that of the ASM specimen. The special rubber membrane was set up covering the pedestal and porous stone prior to the placement of the soil mixture. A hand vacuum was used to suck the air inside the rubber membrane. Then the required amount of dry soil mixture was placed directly on top of the porous stone inside the membrane. The soil mixture was then compacted every 1 cm of height to the desired dry density.

3.2 NUMERICAL ANALYSIS

A two-dimensional (2-D) transient seepage analysis was carried out using Seep/W (Satyanaga et al., 2019b) to assess the pore-water pressure variations within ASM layers of GBS that incorporate different soil mixtures (100ASM, 80SSM, 50SSM) during rainfall. The seepage analysis was conducted under 22 mm/h of rainfall for 24 hours. This rainfall intensity was selected since this value was considered very extreme rainfall and it was used by Public Utilities Board of Singapore to design the drainage in Singapore (Kristo et al., 2019). The boundary conditions of the numerical model are illustrated in Figure 4. The finite element analysis was conducted using 0.25 mm size of element. In this study, a typically steep slope of a 4 m high with an inclination angle of 70° was used in the numerical model (Satyanaga et al., 2019b). The slope was retained by GeoBags filled with ASM and reinforced with geogrids. The original soil behind GBS was simulated based on typical residual soil properties from Old Alluvium in Singapore (Satyanaga and Rahardjo, 2019). The location of groundwater table was assumed at 1 m below the toe of the GBS slope following study by Rahardjo et al. (2018b) for groundwater table distribution in Singapore. Figure 4 shows the slope that was reinforced with the GBS and the geogrids that were strongly attached to GeoBags. The geogrids were extended to 2.8 m (70% of slope height) from GBS facing or 1.4 m behind the coarse RCA layer (Rahardjo et al., 2020). The GBS comprised the compacted residual soil (reinforced zone), geogrids, fine RCA and coarse RCA for the capillary barrier cover, and ASM or SSM for the sustainable green cover. The SWCC and permeability function from each of GBS materials were incorporated in the Seep/W to generate the pore-water pressure profiles for different times (Zhai et al, 2020; 2019). The seepage analysis was conducted under 22 mm/h of rainfall for 24 hours.

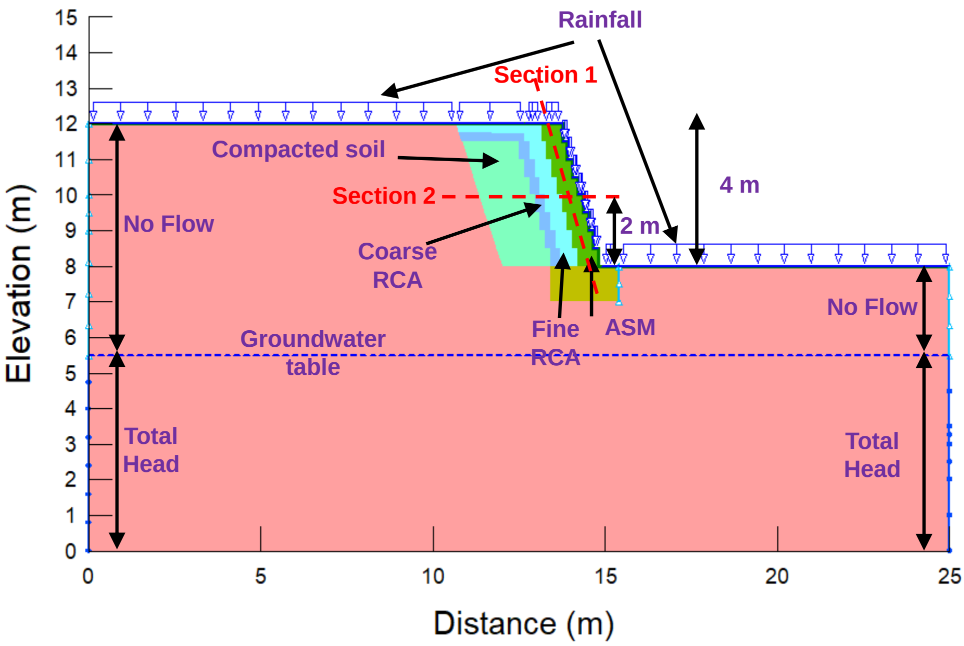

Figure 4. Numerical model for seepage analysis

A deformation analysis was carried out using Sigma/W (Kim et al., 2018) to examine the deformation of an ASM geobag of GeoBarrier System (GBS) that incorporates different percentage of ASM (i.e., 100ASM, 80SSM and 50SSM). The numerical model for the deformation analysis is presented in Figure 5. The application of 70 kPa surcharge at the top of geobag was determined based on the load from 4 m height of GBS as shown in Figure 4. The surcharge was only applied within partial portion of geobag surface since the slope angle of GBS was 70^{o}. The boundary conditions of the numerical model are illustrated in Figure 5. The modulus elasticity, effective cohesion and effective friction angle from ASM and SSM materials were incorporated in the deformation analysis of Sigma/W.

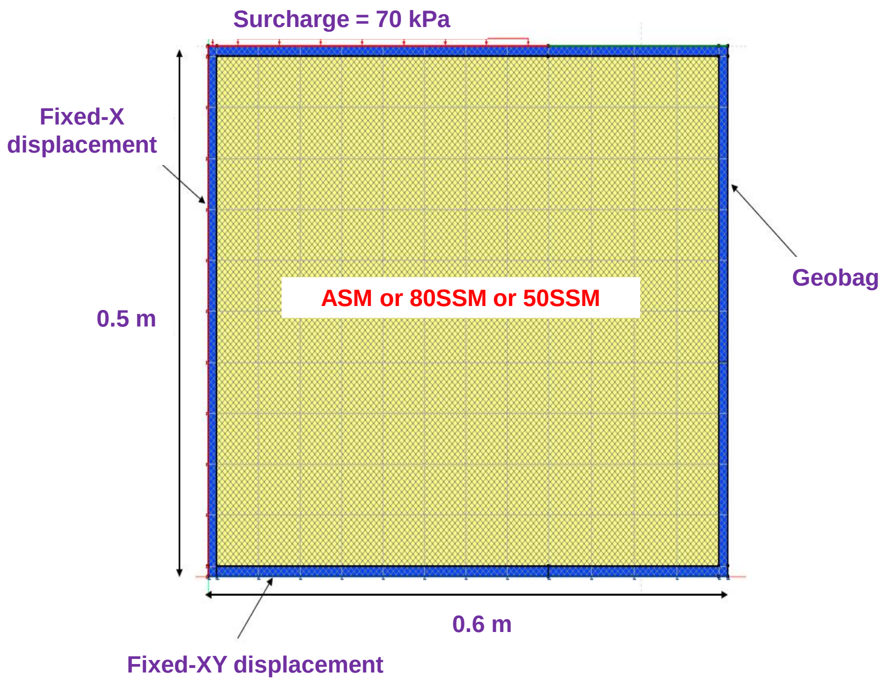

Figure 5. Numerical model for deformation analysis

3.3 LOAD TESTING

Geobags are bags usually made from textiles having high tensile strength and filled with materials such as gravel, sand and even construction wastes. Advantages of soil reinforcement by geobags are summarized as follows (Matsuoka and Liu, 2003): (i) Geobags are light. (ii) Their transportation and relocation are very easy. (iii) Compatibility with the environment because there is no use of any chemicals and there is no noise during construction. (iv) No special or heavy construction equipment is needed. (v) The materials inside Geobags may be any granular remains and construction wastes such as recycled concrete, asphalt, tire and tile.

Xu et al. (2008) utilized plate load testing to estimate the deformation of soil bag. The loading was controlled at a constant rate, about 0.033 kN/s in the unconfined compressive tests. The typical size of soil bags was 10 mm x 40 mm x 40 mm. The soil bags used for unconfined compressive strength tests were made of woven bags in which medium graded sands and gravels were contained. They observed that at failure, soil bags were torn at the points such as contact points with the loading plate, the tailoring points and the maximum distortion points, where the external stress concentrated. Xu et al. (2008) observed that the unconfined compressive strength of soil bags increased linearly with the increase in the tensile strength.

The soil bags containing gravels have larger unconfined compressive strength than the soil bags containing graded sands.

A previous pilot study of GeoBarrier System (Rahardjo et al., 2018) indicated that the ASM Geobags have displayed a noticeable bulging on the front side of the bag, containing the low density ASM. The low density of ASM is required for plant root growth. Therefore, there is a need to improve the deformation issue and study the ASM Geobag with strengthening materials. The loading tests was performed to measure the extent of deformation on ASM and SSM Geobags under different load conditions. The Load Container was lowered onto the Geobag and the Load in the form of a Steel Block was placed inside the Load Container to improve the consistency of the load test results. The Geobag should be restrained from horizontal movement on its three sides (back and two sides) during the load test. The load test was carried out for a minimum duration of 1 hour under the required loading of 75kPa. The deformations of the Geobags were measured in horizontal and vertical directions with an accuracy of at least 1mm.

The loading tests were carried out based on eight (8) sequences. The first step is the setting up of Geobag into a restriction box. The second step involves the filling and compaction of ASM or SSM within the Geobag. The third step is the closing of Geobag by the prefabricated zip. The fourth step is the opening of the front plate of the restriction box. The fifth step includes the lifting and placement of Geobag. The sixth step includes the setting up of the reading station. The seventh step includes the setting up of the steel loading frame and loading container. The eight step consists of the loading test in the field as shown in the schematic diagram of Figure 6.

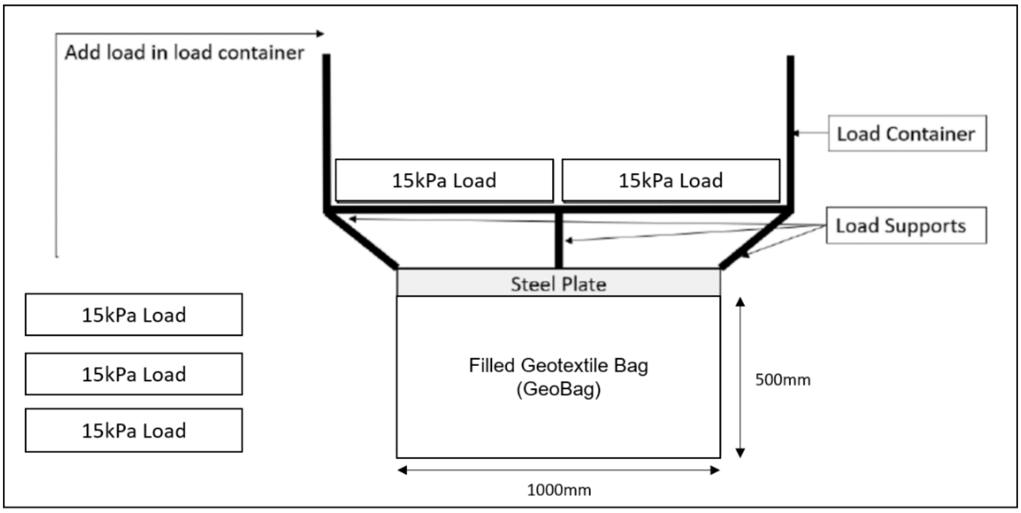

Figure 6. Schematic diagram of loading test

The reading station has been improved to a 3D Scanning Station. A low-cost 3D Scanner was developed to capture the front face deformation of the Geobag, before and after load test was carried out. The developed 3D Scanner with software can replace the reading station process, resulting in time and labour cost savings. The deformation of the Geobag can be measured in horizontal and vertical directions with an accuracy of 1mm. The 3D scanning station is set up 1m away from the front face of the Geobag. The second loading tests were carried out following the same sequences for steps one to five. However, there were different sequences after the fifth steps. The sixth step in the second loading test included the setting up of 3D scanning station. The seventh step includes the setting up of the steel block load. The eight step includes the loading test in the field and its schematic diagram. (Figure 7)

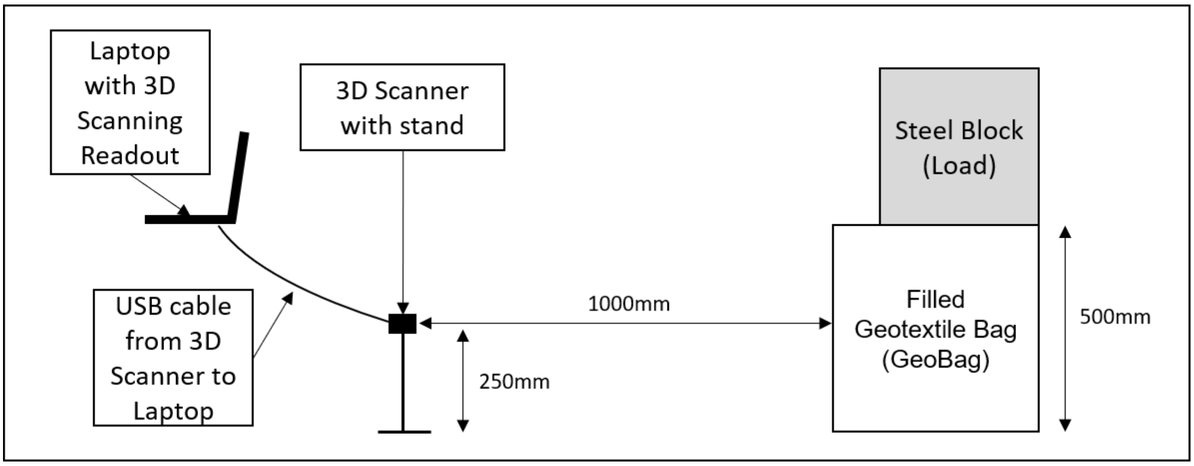

Figure 7. Side Elevation Setup Schematic for the Improved Load Test with 3D scanner

4. RESULTS FROM LABORATORY TESTING, NUMERICAL ANALISIS AND LOAD TESTING

4.1 LABORATORY TESTING

Specific gravity, grain-size distribution and Atterberg limits tests were carried out to determine the index properties of the Approved Soil Mixture (ASM), Structured Soil Mixture (SSM), Fine Recycled Concrete Aggregate (FRCA) and Coarse Recycled Concrete Aggregate (CRCA). Relative density tests were carried out to determine the minimum and maximum void ratio and dry density of FRCA and CRCA. The soil classifications based on the Unified Soil Classification System and results of the index properties tests are presented in Table 1. ASM and 80SSM are classified as clayey sand (SC), CRCA is classified as poorly graded gravel (GP) and 50SSM is classified as Gravel with some percentages of clay material (GC). The grain-size distributions of the investigated materials in this study are presented in Figure 8. The initial conditions associated with dry density and water content of the soil mixtures for all testing are presented in Table 1.

Figure 9 displays the soil-water characteristic curves (SWCC) of the four soil mixtures. The SWCCs of the ASM, 80SSM and 50SSM are all very similar in shape and curvature whereas the SWCC of CRCA has a very steep and sudden drop. The air-entry value (AEV)s of ASM and 80SSM are similar with only a difference of 2kPa. 50SSM has an AEV of 3kPa which is in-between the AEVs of ASM and CRCA. The summary of the AEV and the best fitting parameters are presented in Table 2.

Table 1. Summary of index properties of GBS materials

Soils	ASM	CRCA	FRCA	80SSM	50SSM
Specific gravity, G_s	2.61	NA	2.57	2.6	2.58
Dry density, ρ (Mg/m^3)	1.71	1.92	1.95	1.76	1.82
Water content, w (%)	40	21	25	34	27
Maximum dry density, ρ_{max} (Mg/m^3)	NA	1.76	1.84	NA	NA
Minimum dry density, ρ_{min} (Mg/m^3)	NA	1.17	1.34	NA	NA
Maximum void ratio, e_{max}	NA	1.28	0.91	NA	NA
Minimum void ratio, e_{min}	NA	0.51	0.40	NA	NA
Liquid Limit, LL (%)	36	NA	NA	33	28
Plastic Limit, PL (%)	22	NA	NA	21	17
Plasticity Index, PI (%)	14	NA	NA	12	11
Saturated permeability, k_s (m/s)	1×10^{-6}	2×10^{-2}	1×10^{-5}	3×10^{-5}	6×10^{-4}
Grain Size Distribution - Gravel (%)	5	98.9	0	23	52
Grain Size Distribution - Sand (%)	60	1.1	98	48	29
Grain Size Distribution - Fines (%)	35	0	2	29	19
Unified Soil Classification System	SC	GP	SP	SC	GC

Note: NA = Not applicable

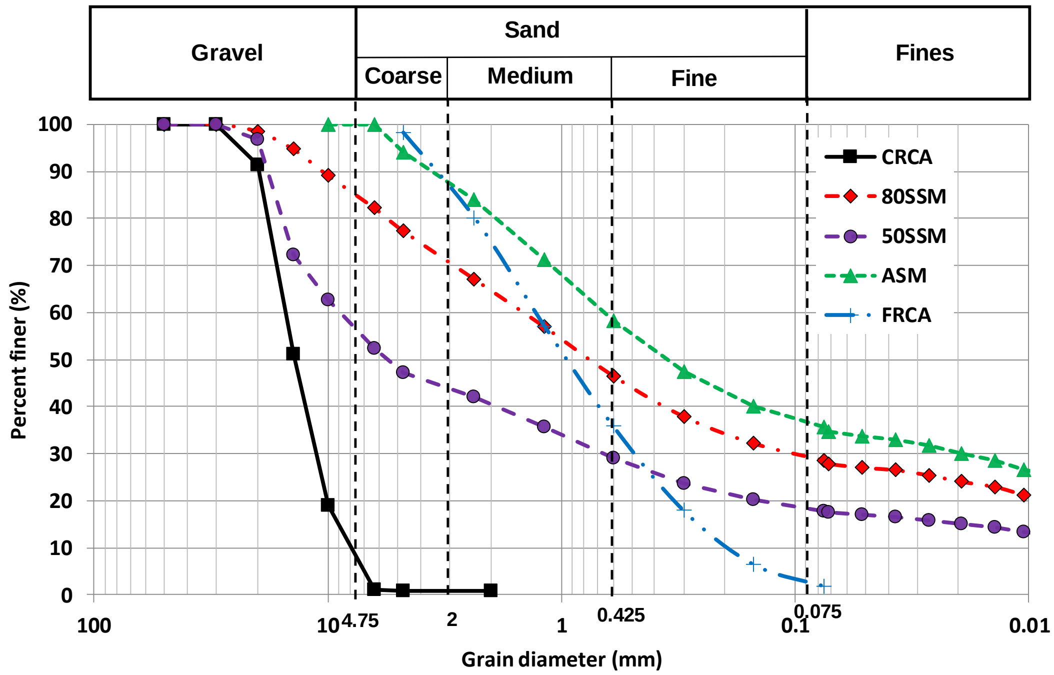

Figure 8. Grain-size distribution of the investigated materials in this study

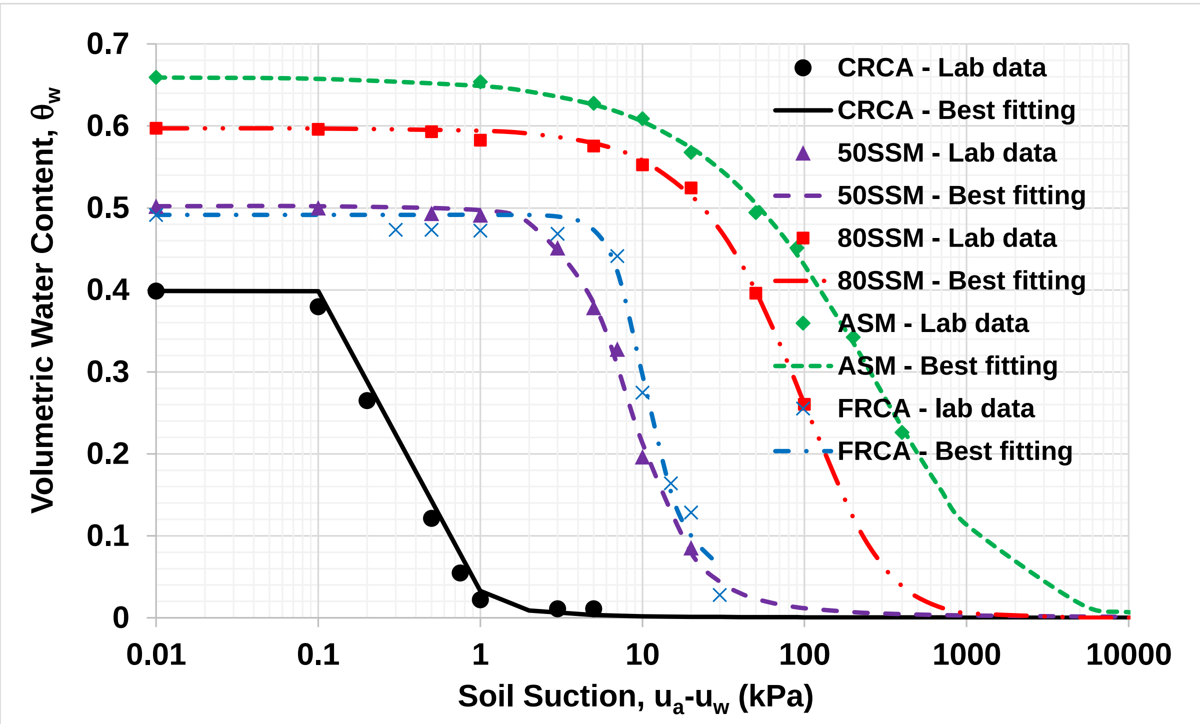

Figure 9. SWCCs of the investigated materials in this study

Table 2. Summary of SWCC parameters

	Symbol	ASM	80SSM	50SSM	CRCA	FRCA
Air-Entry Value (kPa)	Ψ_a	20	18	3	0.1	6
Saturated Volumetric Water Content	θ_s	0.68	0.6	0.5	0.4	0.49
Fredlund & Xing Parameters	a	343	343	17	17	8.7
	n	0.87	0.87	0.98	0.98	4.38
	m	6	6	9.57	9.57	1.22

The permeability functions of the investigated materials are presented in Figure 10. The permeability function of the soil samples increases with an increase in the percentage content of CRCA. Thus, the 80SSM and 50SSM have a greater permeability than ASM, which improves water flow through the soil mixture. Thus, in terms of permeability, the usage of SSM is not detrimental to the GBS. Results from the triaxial test are shown in Table 3.

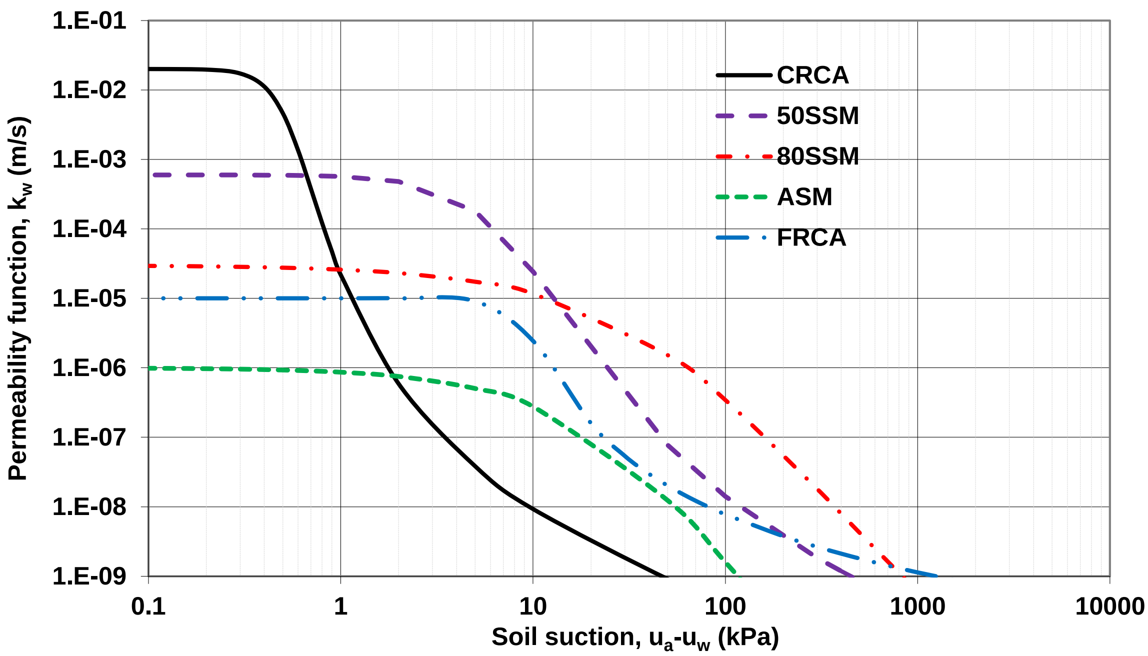

Figure 10. Permeability functions of the investigated materials

Table 3. Summary of shear strength parameters

	Symbol	ASM	80SSM	50SSM	CRCA	FRCA
Effective Cohesion	c' (kPa)	2	5	25	0	0
Effective friction angle	ϕ' (°)	30	44	48	37	34
Unsaturated shear strength	ϕ^b (°)	15	15	13	17	16
Total Unit Weight	γ (kN/m^3)	18	18.5	20	21	20
Modulus Elasticity	E (kPa)	5000	10000	11000	20000	15000

4.2 NUMERICAL ANALYSIS

The pore-water pressure profiles from seepage analyses of Cases 1, 2 and 3 are presented in Figure 11, Figure 12 and Figure 13. The results from Figure 11a, Figure 12a and Figure 13a indicated that high suction values still exist within ASM layers with higher percentages of coarse RCA after 24 hours of rainfall. It shows the 50SSM has a higher performance in maintaining suction during rainfall as compared to 80SSM and 100ASM. The suction will contribute to the additional stiffness of geobag and it will decrease the deformation of geobag. The results from Figure 11b, Figure 12b and Figure 13b indicated the pore-water pressures within Fine RCA and Coarse RCA are similar in trend and magnitude. It shows the different percentages of mixture do not affect the performance of GBS during 24 hours of rainfall.

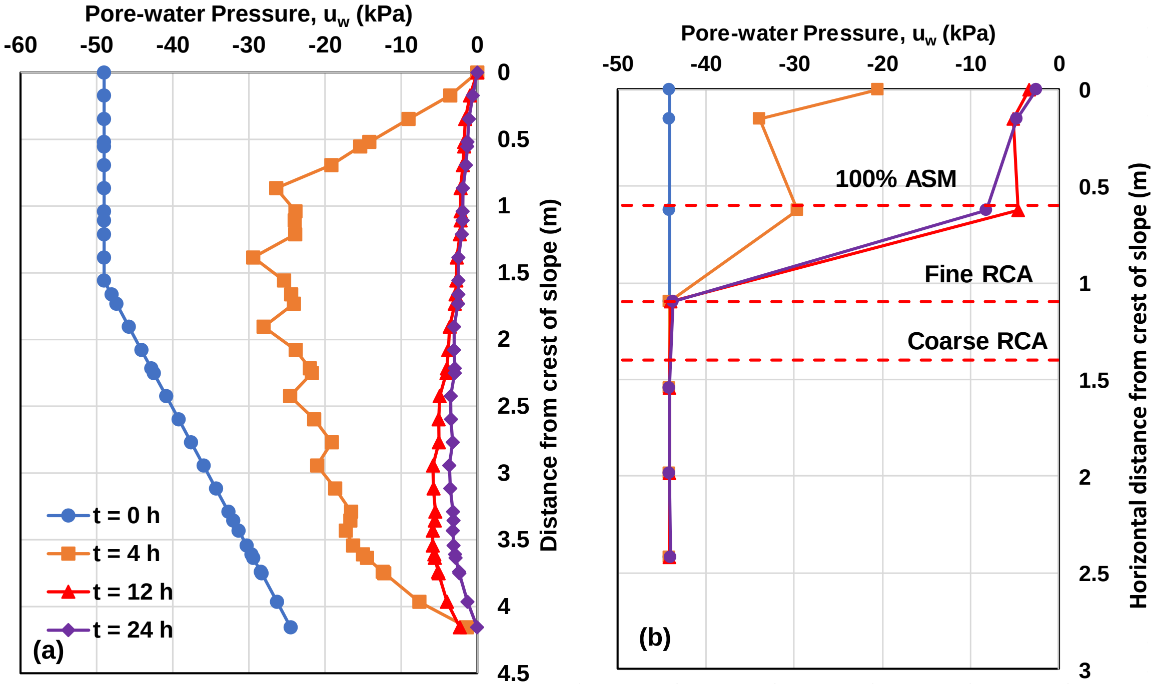

Figure 11. Pore-water pressure profiles from (a) Section 1 (within ASM layer) and (b) Section 2 (at the middle of GBS layer – 2 m depth from the crest of the slope)

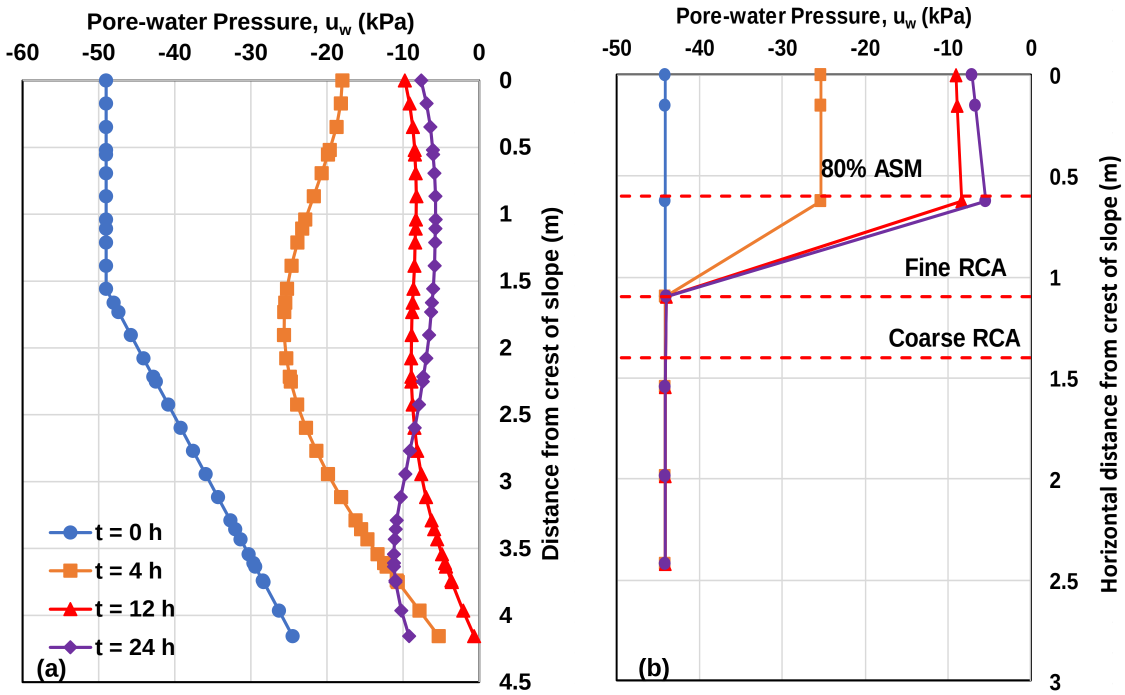

Figure 12. Pore-water pressure profiles from (a) Section 1 (within 80SSM layer) and (b) Section 2 (at the middle of GBS layer – 2 m depth from the crest of the slope)

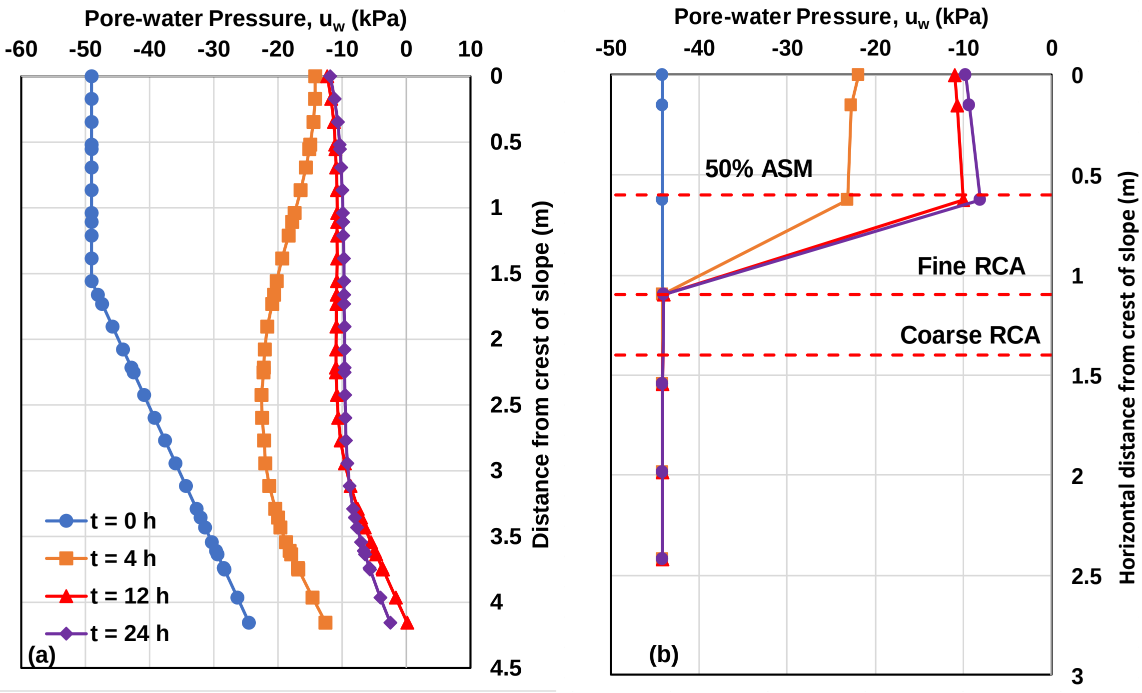

Figure 13. Pore-water pressure profiles from (a) Section 1 (within 50SSM layer) and (b) Section 2 (at the middle of GBS layer – 2 m depth from the crest of the slope)

The results of the numerical analyses of the three cases are presented in Figure 14, Figure 15 and Figure 16. The result from the deformation analysis of case 1 (Figure 14) showed that the maximum horizontal displacement of 58 mm was observed at the side of the ASM bag. The result from the deformation analysis of case 2 (Figure 15) displayed a maximum horizontal displacement of 34 mm. The result from the deformation analysis of case 3 (Figure 16) displayed a maximum horizontal displacement of 16 mm.

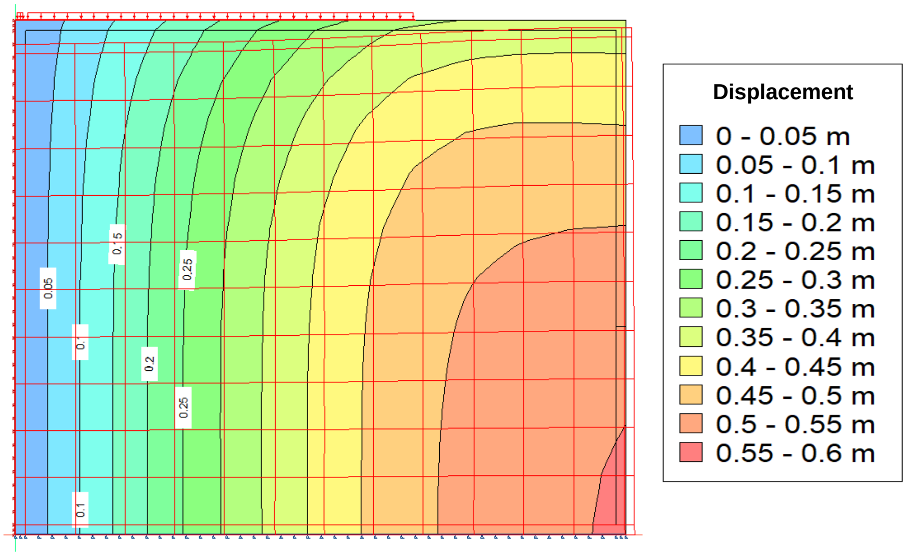

Figure 14. Displacement from deformation analysis of Case 1

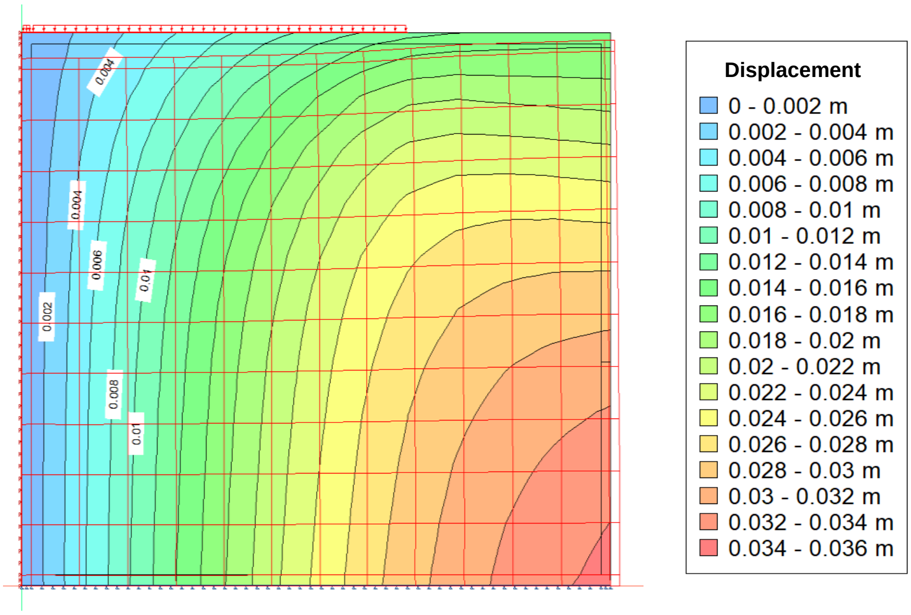

Figure 15. Displacement from deformation analysis of Case 2

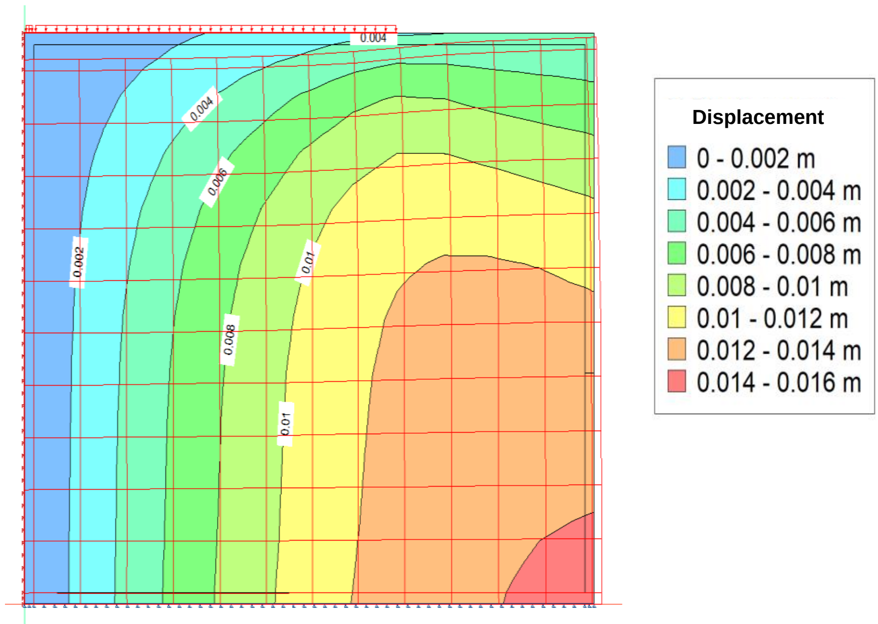

Figure 16. Displacement from deformation analysis of Case 3

4.3 LOAD TESTING

The results from the physical loading test are presented in Figure 17, Figure 18, Figure 19 and Figure 20. The maximum deformations recorded from the loading tests are 55 mm for the ASM Geobag, 28 mm for the 80SSM Geobag and 14 mm for the 50SSM Geobag. The deformation of the geobags decreases with an increase in the coarse RCA content of the soil mixture. There is a strong correlation between the numerical results from the model simulation and the actual physical loading test results, where the Geobags that contain a greater percentage of coarse RCA have smaller deformations. The 50SSM Geobag displays the least deformation.

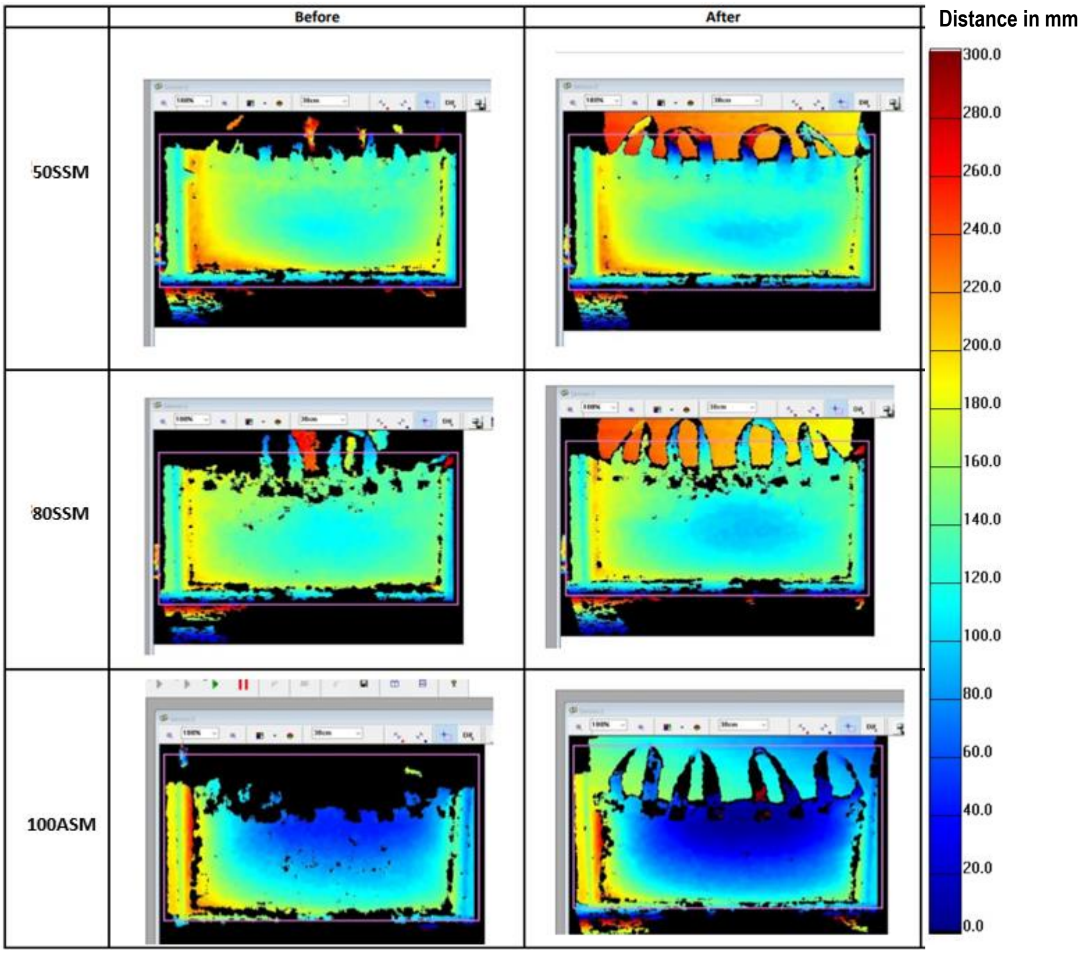

Figure 17. Visual deformation captured by 3D scanner from the physical loading test

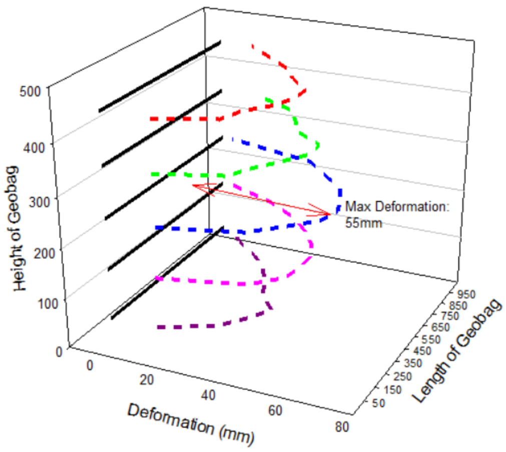

Figure 18. Maximum deformation from loading test on geobag filled with ASM

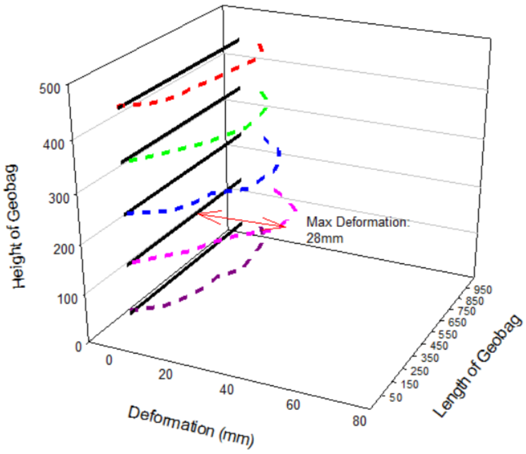

Figure 19. Maximum deformation based on loading test on geobag filled with 80SSM

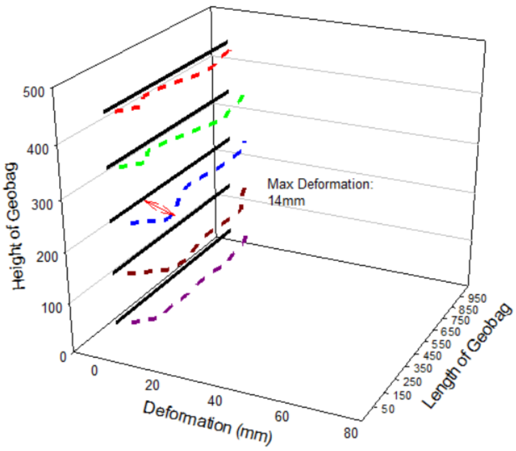

Figure 20. Maximum deformation based on loading test on geobag filled with 50SSM

5. DISCUSSIONS

The results from the grain-size distribution tests indicated that coarse RCA can be classified as poorly-graded gravel (GP). The dry density of coarse RCA is 1.76 Mg/m3 which is similar to the range of dry density of granite chips studied by Rahardjo et al. (2008). Hence, the coarse RCA can be used to replace granite chips in the Structured Soil Mixture (SSM). Further investigation is carried out to investigate the unsaturated characteristics of coarse RCA as compared to granite chips to be used within SSM. The hydraulic properties and shear strength of coarse-grained soil mixture were investigated by Rahardjo et al. (2008). The soil–water characteristic curve parameters such as air-entry value and residual volumetric water content of the soil mixture were found to have decreased with an increase in the granite chip contents. From tests conducted, it was found that coarse RCA soil mixtures also showcased similar properties with regards to their soil-water characteristic curve parameters.

From Table 2, it can be seen that the air-entry value and saturated volumetric water content decreases with an increase in the percentage content of coarse RCA in the soil mixture. From Rahardjo et al. (2008), the saturated permeability of the granite chip soil mixture was found to have increased greatly when the percentage of granite chips in the soil mixture exceeded 50%. From the results of the triaxial test conducted as shown in Table 3, coarse RCA soil mixtures also displayed an increase in saturated permeability with an increase in coarse RCA percentage. Thus, since both granite chips and coarse RCA present similar hydraulic characteristics, coarse RCA can be used to replace granite chips for use in SSM.

The results from the Geobag stress-strain analysis of case 1, 2 and 3 (Figure 14, Figure 15, Figure 16) show that with an increase in the percentage of coarse RCA in the SSM, the lower the deformation experienced by the Geobag. This is corroborated by the results from the physical loading test (Figure 18, Figure 19, Figure 20) which follow the same relationship between coarse RCA percentage and level of deformation. The maximum displacement from the stress-strain analysis Case 3 is 16 mm which is close to the maximum displacement from the physical loading test (14 mm). The maximum displacement from stress-strain analysis Case 2 is 36 mm which is close to the maximum displacement from the physical loading test (28 mm). The maximum displacement from the stress-strain analysis Case 1 is 60 mm which is close to the maximum displacement from the physical loading test (55 mm). The results are further supported by Rahardjo et al. (2009)who observed that a mixture of 50% topsoil and 50% granite chip provided the highest resistance against the wind force needed to uproot a tree as indicated by their static analysis and numerical modelling. They found that an increase in percentage of granite content brings about an increase in the resistance to uprooting till a maximum optimum point. The same ratio of 50% ASM and 50% coarse RCA was proposed to be used in the SSM geobag to provide improved resistance to deformation.

From the study of unsaturated soil properties, the permeability of the SSM was found to be greater than ASM. This characteristic, k_w, has no impact on the deformation of the Geobag. Figures 11 to 13 indicated that the suctions within coarse RCA were maintained during 24 hours of rainfall. It shows that the soil mixtures do not hinder the water flow and the suctions behind the GBS can be maintained during heavy rainfall.

In summary, from the analysis and actual loading tests, it can be concluded that the 50SSM has the best performance with respect to deformation while still maintaining sufficient permeability as well as AEV. The deformation from the stress-strain analysis Case 1 (50SSM) is less than or equal to the allowable deformation of GBS wall (16 mm) (Rahardjo et al., 2019b). Therefore, the use of Structured Soil Mixture (SSM) in GBS is recommended over ASM.

6. CONCLUSIONS

Based on the study presented in this paper, the following conclusions can be drawn from this study:

- Coarse RCA can be used to replace granite chips in the structural soil.
- The air-entry value and saturated volumetric water content decrease with an increase in the percentage content of coarse RCA in the soil mixture.
- The results from the loading test and stress-strain analyses indicated that the soil mixture with a ratio of 50% ASM and 50% coarse RCA can be used in the SSM geobag to provide improved resistance to deformation of GBS.
- The results from the seepage analyses indicated that the soil mixtures do not hinder the water flow and the suctions behind the GBS can be maintained during heavy rainfall.
- The permeability of the SSM was found to be greater than ASM which can be used in supporting plant life within GBS.

REFERENCES

AASHTO. 2012. LRFD Bridge Design Specifications 6th ed. American Association of State Highway and Transportation Official. Washington, DC.

ASTM D7830/D7830M-13. 2013. Standard Test Method for In-Place Density (Unit Weight) and Water Content of Soil Using an Electromagnetic Soil Density Gauge. ASTM International, West Conshohocken, PA.

ASTM D698-12. 2012. Standard Test Methods for Laboratory Compaction Characteristics of Soil Using Standard Effort. ASTM International. West Conshohocken, PA.

ASTM D2487-11. 2011. Standard Practice for Classification of Soils for Engineering Purposes (Unified Soil Classification System). ASTM International. West Conshohocken, PA.

ASTM D6913-04. 2009. Standard Test Method for Particle-Size Distribution (Gradation) of Soils using Sieve Analysis. ASTM International, West Conshohocken, PA.

ASTM D7181-11. 2009. Method for Consolidated Drained Triaxial Compression Test for Soils. ASTM International, West Conshohocken, PA.

ASTM D4767-04. 2009. Test method for consolidated undrained triaxial compression test for cohesive soils. ASTM International. West Conshohocken, PA.

ASTM D7181-11. 2009. Method for Consolidated Drained Triaxial Compression Test for Soils. ASTM International, West Conshohocken, PA.
ASTM D6838-02. 2008. Standard Test Methods for Determination of the Soil Water Characteristic Curve for Desorption Using Hanging Column, Pressure Extractor, Chilled Mirror Hygrometer, or Centrifuge. ASTM International, West Conshohocken, PA.
ASTM D4253-00. 2006. Standard Test Methods for Maximum Index Density and Unit Weight of Soils Using a Vibratory Table. ASTM International, West Conshohocken. PA
ASTM D 4318–00. 2000. Standard Test Methods for Liquid Limit, Plastic Limit, and Plasticity Index of Soils. ASTM International, West Conshohocken, PA.
ASTM D 854-02. 2002. Standard Test Methods for Specific Gravity of Soil Solids by Water Pycnometer. ASTM International, West Conshohocken, PA
ASTM D 1140-00. 2002. Standard Test Methods for Amount of Material in Soils Finer than the No.200 (75-μm) Sieve. ASTM International, West Conshohocken, PA
Aung, K., Rahardjo, H., Leong, E. C., and Toll, D. G. (2001). "Relationship between porosimetry measurement and soil—water characteristic curve for an unsaturated residual soil." Unsaturated Soil Concepts and Their Application in Geotechnical Practice, Springer, 401-416.
Childs, E.C. and Collis-George, N (1950) "The permeability of porous 422 materials."Proc. Roy Soc. A201, 392-405
Dye, H., Houston, S., and Welfert, B. (2011). "Influence of unsaturated soil properties uncertainty on moisture flow modeling." Geotechnical and Geological Engineering, 29(2), 161-169.
Fredlund, D. G. (2006). Unsaturated Soil Mechanics in Engineering Practice. Journal of Geotechnical and Geoenvironmental Engineering, 132(3), 286-321.
Fredlund, D. G., & Xing, A. (1994). Equations for the soil-water characteristic curve. Canadian Geotechnical Journal, 31(4), 521-532.
Fredlund, D. G., & Rahardjo, H. (1993). Soil mechanics for unsaturated soils. New York: John Wiley and Sons Inc.
Fredlund, D. G., & Morgenstern, N. R. (1977). Stress state variables for unsaturated soils. Journal of Geotechnical Engineering Division, ASCE, 103(GT5), 447–466.
Fredlund, D. G., Morgenstern, N. R., & Widger, R. A. (1978). The Shear Strength of Unsaturated Soils. Canadian Geotechnical Journal, 15(3), 313-321.
Gasmo, J. M., Rahardjo, H., & Leong, E. C. (2000). Infiltration effects on stability of a residual soil slope. Computers and Geotechnics, 26(2), 145-165.
Harnas, F.R., H. Rahardjo., E.C. Leong, and J.Y. Wang (2016) "Physical Model for the Investigation of Capillary Barriers Performance Made Using Recycled Asphalt", Geotechnical Testing Journal, ASTM International, November, Vol 39, issue 6, pp.977-990.
Holden, P. A., & Fierer, N. (2005). Microbial processes in the vadose zone. Vadose Zone Journal, 4(1), 1-21.
Holsworth, L. (2014). Numerical analysis of vegetation effects on slope stability. (Master's thesis), Universität für Bodenkultur, Vienna.
Hoyos, L.R. (1998). "Experimental and Computational Modeling of Unsaturated Soil Behavior Under True Triaxial Stress States." Ph.D. Dissertation, Georgia Institute of Technology, Atlanta, GA
Khire, M., Benson, C., and Bosscher, P. 2000. Capillary Barriers: Design Variables and Water Balance, Journal of Geotechnical and Geoenvirnmental Engineering., ASCE 126(8): 695-708.

Kristo, C., Rahardjo, H. and Satyanaga, A. (2019) “Effect of Hysteresis on The Stability of Residual Soil Slope”. International Soil and Water Conservation Research. September 2019. Vol. 7, pp. 226-238.

Leong, E. C., & Rahardjo, H. (1997a). Permeability functions for unsaturated soils. Journal of Geotechnical and Geoenvironmental Engineering, 123(12), 1118-1126.

McCulloch, T., Kang, D., Shamet, R., Lee, S.J. and Nam, B.H. (2017). “Long-Term Performance of Recycled Concrete Aggregate for Subsurface Drainage.” J. Performance of Constructed Facilities, 31(4), 47-54.

Mualem, Y. (1976). A new model for predicting the hydraulic conductivity of unsaturated porous media. Water Resources Research, 12(3), 513-522.

Rahardjo, H., Kim, Y., Gofar, N., Satyanaga, A. (2020). Analyses and design of steep slope with GeoBarrier system (GBS) under heavy rainfall. Geotextiles and Geomembranes, Vol. 48, pp. 157-169.

Rahardjo, H., Satyanaga, A., Gofar, N., Leong, E.C., Kew, J.H., Wang, C.L., Wong, J.L.H. (2019a). “Geobarrier System for Protection against Rainfall-induced Slope Failure” ISSMGE International Journal of Geoengineering Case Histories. Vol. 5, No. 1, pp. 26-42.

Rahardjo, H., Gofar, N., Satyanaga, A., Leong, E.C., Wang, C.L., Wong, J.L.H. (2019b). “Effect of Rainfall Infiltration on Deformation of Geobarrier”, Geotechnical and Geological Engineering, Vol. 37, pp. 1383-1399.

Rahardjo, H., N. Gofar, F. Harnas and A. Satyanaga (2018) “Effect of Geobags on Water Flow through Capillary Barrier System”, Geotechnical Engineering Journal of the SEAGS & AGSSEA, December, Vol 49, No 4, pp. 1-6.

Rahardjo, H., S. Krisnanto, and E.C. Leong (2016a) “Effectiveness of Capillary Barrier and Vegetative Slope Covers in Maintaining Soil Suction”, Soils and Rocks Journal, Special topic on Theory and Practice of Unsaturated Soils Mechanics, January-April, Vol.39(1), pp.51-69

Rahardjo, H., A. Satyanaga, F.R. Harnas, and E.C. Leong (2016b) “Use of Dual Capillary Barrier as Cover System for a Sanitary Landfill in Singapore”, Indian Geotechnical Journal, September, Vol.46, issue 3, pp 228-238.

Rahardjo, H., V.A. Santoso, E.C. Leong, Y.S. Ng, C.P.H. Tam and A. Satyanaga (2013). “Use of Recycled Crushed Concrete and Secudrain in Capillary Barrier for Slope Stabilization”. Canadian Geotechnical Journal, June, Vol. 50, pp. 1-12.

Rahardjo, H., Satyanaga, A., Leong, E.-C., Ng, Y. S., and Pang, H. T. C. (2012). "Variability of residual soil properties." Engineering Geology, 141, 124-140.

Rahardjo, H., Krisdani, H., Leong, E.C., Ng, Y.S., Foo, M.D. and Wang, C.L. 2007. Capillary Barrier as Slope Cover. Proc. 10th Australia New Zealand Conference on Geomechanics “Common Ground”. Brisbane, Australia, 21-24 October, 2: 698 - 703.

Satyanaga, A., Rahardjo, H., Hua, C.J. (2019). “Numerical simulation of capillary barrier system under rainfall infiltration” ISSMGE International Journal of Geoengineering Case Histories. 5(1):43-54.

Satyanaga, A., Rahardjo, H., Leong, E.-C., and Wang, J.-Y. (2013). "Water characteristic curve of soil with bimodal grain-size distribution." Computers and Geotechnics, 48, 51-61.

Tami, D., Rahardjo, H., and Leong, E.-C. (2004). "Effects of hysteresis on steady-state infiltration in unsaturated slopes." Journal of Geotechnical and Geoenvironmental Engineering, 130(9), 956-967.

Terzaghi, K. (1936) "The shear strength of saturated soils." Proc., Proc. 1St Int. Conf. Soil Mech. Found. Eng.(Cambridge, MA), 54-56.

Vanapalli, S. K., Fredlund, D. G., Pufahl, D. E., & Clifton, A. W. (1996). Model for the prediction of shear strength with respect to soil suction. Canadian Geotechnical Journal, 33(3), 379-392.

Zhai, Q., Rahardjo, H., Satyanaga, A., Dai, G. and Zhuang, Y (2020) “Framework to estimate the soil-water characteristic curve for soils with different void ratios” Bulletin of Engineering Geology and the Environment (Accepted in Apr 2020) https://doi.org/10.1007/s10064-020-01825-8

Zhai, Q., Rahardjo, H., Satyanaga, A. (2019a) “Estimation of the air permeability function from the Soil-Water Characteristic Curve”, Canadian Geotechnical journal, Vol. 56, No. 4, pp. 505-513.

Zhai, Q., H. Rahardjo, A. Satyanaga, Priono and G. Dai (2019b). "Role of the pore-size distribution function on water flow in unsaturated soil" Journal of Zhejiang University-SCIENCE A, January, Vol. 20, No. 1, pp. 10-20.

Zhai, Q., Rahardjo, H., and Satyanaga, A. (2016). "Variability in unsaturated hydraulic properties of residual soil in Singapore." Engineering geology, 209, 21-29

Zhan, TLT, Li, H, Jia, GW, Chen, YM and Fredlund, DG (2014). “Physical and numerical study of lateral diversion by three layer inclined capillary barrier covers under humid climatic conditions.” Canadian Geotechnical Journal, 51(12), 1438-1448.